Diffusion and Seed Shape: Intertwined Parameters in the Synthesis of Branched Metal Nanostructures

Rebecca G. Weiner,[†] Christopher J. DeSantis,[†] Mariana B. T. Cardoso,[‡] and Sara E. Skrabalak[†,*]

[†]Department of Chemistry, Indiana University, Bloomington, Indiana 47405, United States and [‡]Instituto de Química, Departamento de Química Fundamental Av Prof Lineu Prestes, Universidade de São Paulo, 748 São Paulo, São Paulo 05508000, Brazil. The manuscript was written through contributions of all authors. All authors have given approval to the final version of the manuscript.

ABSTRACT Branched nanocrystals display interesting optical and catalytic properties on account of their high surface areas and tips with small radii of curvatures. However, many synthetic routes toward branched nanocrystals result in inhomogeneous samples on account of asymmetric branching. Seed-mediated coreduction is a recently developed route to symmetrically branched nanocrystals where the symmetry of the seeds is transferred to the final stellated morphologies. Here, general guidelines to stellated nanocrystals are outlined by surveying coreduction of Au and Pd precursors in the presence of a variety of shape-controlled Au seeds to achieve Au/Pd nanostructures. Single-crystalline, twinned, and anisotropic seeds were analyzed to expand the classes of stellated nanostructures synthetically accessible. Significantly, single-crystalline Au seeds adopt {100}-terminated intermediates prior to branching, regardless of initial seed shape. We compared these results with those obtained with shape-controlled Pd seeds, and seed composition was identified as an important synthetic parameter, with Pd seeds being more resistant to shape changes during overgrowth. This difference is attributed to the greater diffusion rate of Au atoms on Au seeds compared to Au atoms on Pd seeds. These results provide guidelines for the seeded synthesis of symmetrically branched nanocrystals and architecturally defined bimetallic nanostructures in general.

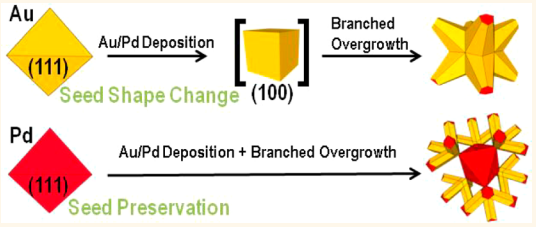

KEYWORDS: nanostars · gold · palladium · LSPR · nanorods · bimetallic

Metal nanostructures are of interest due to their unique properties that depend on crystallite size, shape, and composition.[1−5] Recently, this interest has extended to bimetallic nanostructures on account of their nanoscale properties, which arise not just from structural parameters such as size and shape but also on the nature of the bimetallic distribution itself.[6−12] Such structures are promising multifunctional platforms;[13] however, routes to bimetallic nanomaterials where their structure and composition are precisely controlled are needed. As one example, seed-mediated coreduction (SMCR) was demonstrated as a route to symmetrically branched Au/Pd nanostructures, where the stellated Au-based profile provides a well-defined localized surface plasmon resonance (LSPR) despite the incorporation of the poor plasmonic metal Pd.[14] Through such architectural design, the optical properties of nanoscale Au are integrated with the chemical properties of nanoscale Pd.[15] In SMCR, two metal precursors are coreduced to deposit two metals onto shape-controlled metal seeds. This technique addresses the challenges of traditional coreduction routes to bimetallic nanostructures by coupling them with the advantages of seed-mediated methods. Expansion of the classes of bimetallic nanocrystals (NCs) synthesized by SMCR will provide greater understanding of the nanoscale properties that emerge from coupling nanoarchitecture with composition;[15−17] however, questions remain that preclude broad application of SMCR. Thus, this manuscript reports guidelines for the design of multifunctional branched NCs synthesized by SMCR.

Previously, using shape-controlled Au or Pd NCs as seeds, symmetrically branched Au/Pd NCs were synthesized by SMCR.[18] These particles display interesting optical[19] and catalytic properties.[14] From initial studies of SMCR with Au seeds, determining the symmetry relationships between the Au seeds and the final branched NCs was

* Address correspondence to sskrabal@indiana.edu.

Received for review June 24, 2014 and accepted August 12, 2014.

Published online August 18, 2014
10.1021/nn5034345

difficult. This challenge arose because Au deposits predominantly first onto the Au seeds. To better understand these symmetry relationships, coreduction of Au and Pd precursors was performed in the presence of Pd seeds. The Pd seeds serve as transmission electron microscopy (TEM)-labels analogous to fluorophore labeling in confocal microscopy.[20] Scanning transmission electron microscopy (STEM) coupled with energy dispersive X-ray spectroscopy (EDX) for elemental mapping was implemented to correlate seed structure to the symmetry of the branched overgrowth. Studies with various shape-controlled Pd NCs concluded that overgrowth initiates preferentially at features of highest energy, such as seed vertices, with branches extending in ⟨111⟩ directions in the absence of twin planes. For example, coreduction of Au and Pd precursors in the presence of octahedral Pd seeds produced four branches on each vertex, resulting in 24-branched particles with O_h symmetry.[21]

However, the assumption that growth occurs primarily at features of highest energy is likely oversimplified due to factors such as surface diffusion rates and seed crystallinity, and these factors could be intertwined. This complexity is evident from comparing results obtained with similarly shaped seeds of different compositions. For example, when Au and Pd precursors are coreduced to deposit metal onto quasi-octahedral Au seeds, 8-branched octopodal structures with O_h symmetry form, whereas 24-branched particles with O_h symmetry form from octahedral Pd seeds as previously described.[21] Yet when either Au (this manuscript) or Pd nanocubes[21] are used as seeds, octopods with O_h symmetry form.

In this manuscript, experiments are presented which elucidate the roles of seed shape and composition in the synthesis of branched NCs by SMCR. In particular, Au seeds adopt new shapes prior to branch growth more facilely than Pd seeds during SMCR due to differences in surface diffusion rates of deposited metal on seeds with different compositions. Although the instability of Au seeds could limit the branching patterns accessible *via* SMCR, expanding the seed shapes used with SMCR provides access to new stellated structures. Together, these results provide guidelines toward the synthesis of new branched and bimetallic NCs *via* SMCR and seeded methods in general.

RESULTS AND DISCUSSION

To determine the roles of seed shape and composition, Au and Pd single-crystalline, anisotropic, and twinned shape-controlled NCs were systematically used as seeds with SMCR in a model Au−Pd system. The structural differences between branched overgrowth on Au and Pd seeds were than compared to determine the symmetry relationships between seeds and final branched structures and to establish general guidelines for applying SMCR toward the synthesis of new nanostructures.

Coreduction with Au and Pd Cubes, Octahedra and Rhombic Dodecahedra as Seeds. To evaluate the possibility for differences in adatom diffusion rates on seeds with different compositions, SMCR of Au and Pd precursors was performed in the presence of either Au or Pd single-crystalline NCs. As Au atoms deposit primarily first onto seeds during SMCR, the surface diffusion rates of Au adatoms should differ depending on whether Au or Pd seeds are being used.[22] These differences could account for the different branched structures obtained with quasi-octahedral Au seeds compared to Pd octahedra. Typically, self-diffusion is more rapid due to lattice and electronic match.[23] Thus, Au adatoms would diffuse more rapidly on Au seeds than on Pd seeds and adopt new shapes more facilely. Single-crystalline seed shapes analyzed include: {100}-terminated nanocubes, {110}-terminated rhombic dodecahedra, and {111}-terminated octahedra. For face-centered cubic (FCC) metals such as Au and Pd, {111}, {100} and {110} are the lowest energy facets and thus most stable.[1] Therefore, these seeds were chosen to survey the most commonly encountered shapes in Au and Pd NC systems and establish the symmetry relationships between NC seeds and branched NCs after SMCR.

Coreduction of Au and Pd precursors to deposit metal onto Au nanocubes[24] resulted in 8-branched O_h structures (Figure 1A, B). From STEM-EDX and TEM analysis, Au (shown in yellow in EDX mapping) was found to deposit primarily on the octahedral Au seeds, followed by branched overgrowth. Pd (shown in red in EDX mapping) predominates on the surfaces of structures and at branch tips (Figure S1A−D, Supporting Information). Coreduction of Au and Pd precursors to deposit metal onto cubic Pd seeds was previously reported[21] and also resulted in octopodal structures with O_h symmetry conserved. In the previous report, elemental mapping revealed that the cubic Pd seeds were intact and do not undergo structural changes during overgrowth.[21] Au deposits primarily first followed by Pd localization at the tips and on the exterior of the particles. In both cases, electron diffraction verifies that one branch grows off each vertex of the cubes and extends in a ⟨111⟩ direction because when the particle is oriented with four branches toward a surface, the [100] zone axis is displayed and [111] is displayed when looking down one branch (Figure S1E, F, Supporting Information). Comparisons of Au and Pd seeds indicate the branched growth initiates at seed vertices, resulting in 8-branched octopods.

Coreduction of Au and Pd precursors to deposit metal onto similarly sized Au and Pd octahedra[14,21] was also performed. From octahedral Au seeds, 8-branched Au/Pd octopods with O_h symmetry formed (Figure 1C, D). These structures are similar to those obtained from either quasi-octahedral Au or cubic Au seeds, where electron diffraction indicated that the branches grow in ⟨111⟩ directions. However, slight

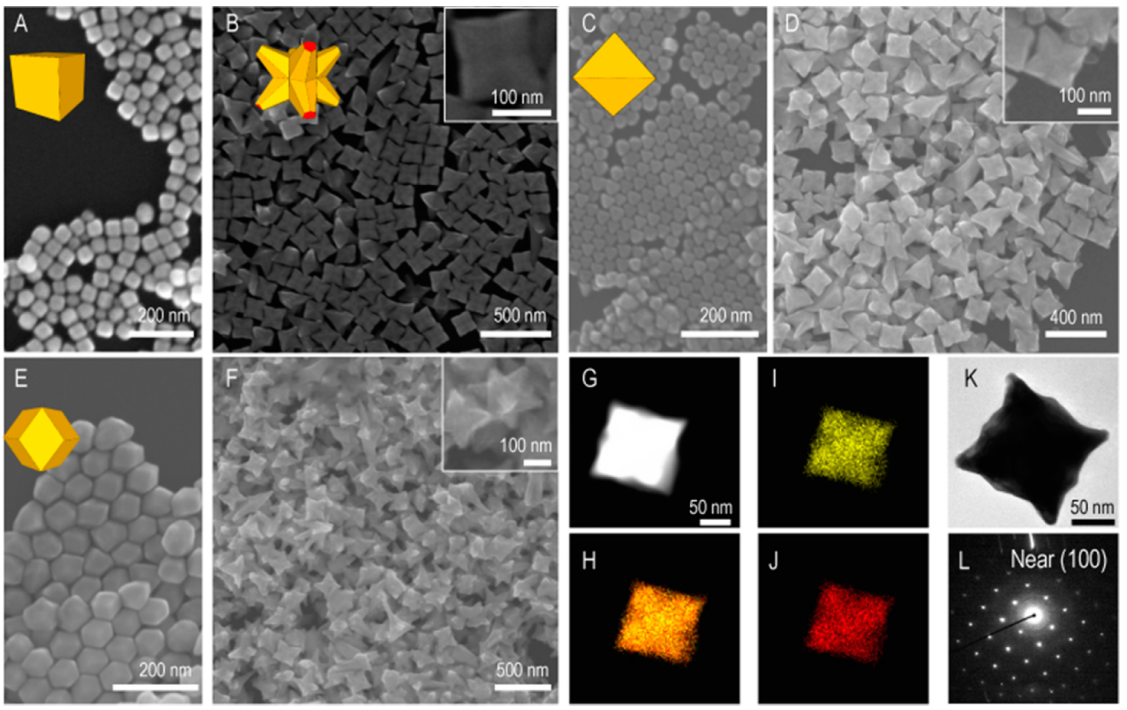

Figure 1. (A) SEM of cubic Au seeds. (B) SEM of Au/Pd octopods from cubic Au seeds. (C) SEM of octahedral Au seeds. (D) SEM of Au/Pd octopods from octahedral Au seeds. (E) SEM of rhombic dodecahedral Au seeds. (F) SEM of Au/Pd octopods from rhombic dodecahedral Au seeds. (G) STEM on an individual octopod built from a rhombic dodecahedral Au seed. (H–J) STEM-EDX elemental mapping of corresponding octopod where Au is represented by yellow and Pd is red; (H) is an overlay of Au and Pd signals, shown separately in (I) and (J). (K,L) TEM and corresponding electron diffraction of Au/Pd octopod from rhombic dodecahedral Au seeds.

differences in branch length and tip thickness are evident and likely arise from differences in seeds sizes (and thus surface area for metal deposition) from one shape to the next. STEM-EDX and TEM analysis indicates that Pd concentrates on the tips of the nanostructures and Au localizes in the interior of the particles due to the Au precursor reducing primarily first followed by Pd deposition. Au from the octahedral seed and Au from the overgrowth are indistinguishable. Therefore, determining where the branches initiate relative to the seed is difficult, but clearly the number of branches is inconsistent with the number of vertices of the octahedral seeds (8 branches *versus* 6 vertices). Interestingly, previous work found that octahedral Pd seeds yielded a more complex branching pattern.[21] After coreduction of Au and Pd precursors to deposit metal onto octahedral Pd seeds, the NCs have 24 branches and O_h symmetry conserved from the octahedral seed. The final morphology of the particle was determined from scanning electron microcopy (SEM) tilt studies, which revealed that four branches grow off of each vertex in ⟨111⟩ directions. Similar to the octahedral Au seeds, Au deposited primarily first and Pd localized on the exterior of the particles and at branch tips.

These results suggest that Au seeds can adopt new shapes during SMCR before branch growth, where the Au octahedra may adopt a cubic profile during overgrowth, prior to branch formation. In fact, we previously speculated the formation of cubic intermediates from quasi-octahedral seeds but were unable to trap the structure.[14] However, by using bis(*p*-sulfonatophenyl)phenylphosphine dihydrate dipotassium (BSPP) salt to quench the overgrowth process, products can be isolated for characterization with greater time resolution.[20] In some syntheses, BSPP was used to manipulate reaction conditions. For example, BSPP can coordinate to Ag^+, facilitating a change in the amount of metal available for growth and in turn the aspect ratio of the nanoplates.[25] Thus, to ensure that BSPP is not responsible for changes in seed and nanocrystal shapes in our experiments, BSPP was added to an aqueous solution containing Au octahedral seeds. First, Au octahedra were added to 25 mL of water (in place of the typical growth solution). An aliquot of this seed solution was then added to BSPP solution, just as reaction aliquots were treated. After collection, no differences in morphology were observed when comparing the initial and final octahedra (Figure S2, Supporting Information). The results from this control experiment, along with preservation of anticipated product shape with BSPP addition, validate the use of BSPP to quench the SMCR process. In Figure 2A–D are SEM images of the octahedral seeds and structures present at 1, 2, and 3 min following the addition of seeds. Interestingly, at 3 min, cubic intermediates were captured. The growth solution contains a high concentration of Br^- from

cetyltrimethylammonium bromide (CTAB), which is known to stabilize {100} facets of FCC metals.[26] Other halide impurities, such as I^-, are often present in CTAB and can contribute to morphology development. However, previous studies decoupled the roles of, Cl^-, Br^-, and I^- to morphology development in this system, with the octopodal morphology preserved at low concentrations I^- and Br^-.[27] Hence, a {100}-terminated cube would be a favored intermediate in this system, although octopods are also obtained in the absence of Br^-.[18] In general, overgrowth of Au seeds has led to a variety of shape-controlled Au NCs.[28−31] Thus, octahedral Au seeds transform in the earliest stages of SMCR to adopt a cubic structure before branch formation, as summarized by Scheme 1. Analysis with STEM-EDX confirmed that this intermediate was Au and no Pd signal above background was recorded, indicating that the octahedral seeds transform into cubes prior to branch growth. In contrast, Pd octahedra do not adopt a cubic intermediate during SMCR, and this distinction explains the different branching patterns obtained with Au and Pd octahedral seeds.

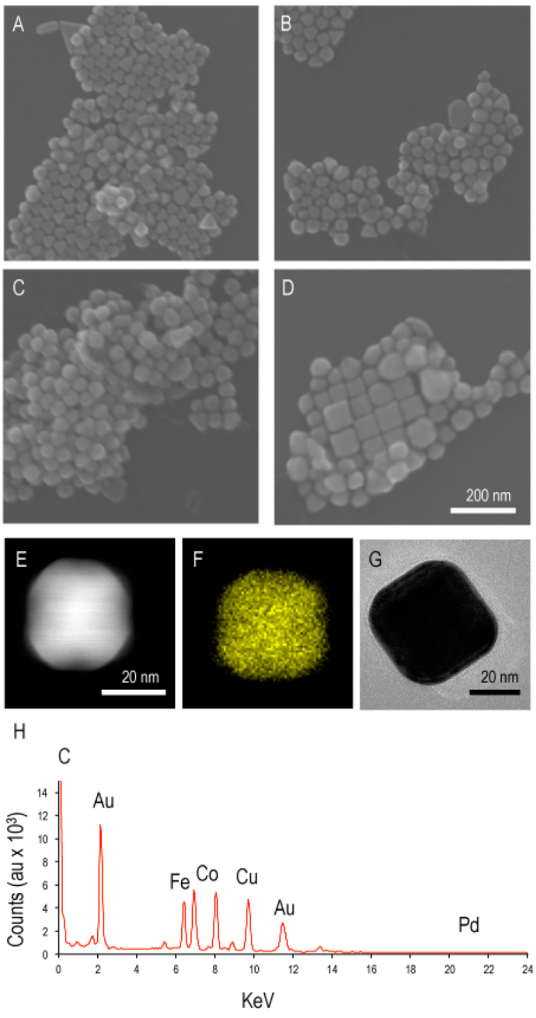

Figure 2. (A−D) SEM images of product produced as a function of time with octahedral Au seeds: (A) 0 min, (B) 1 min, (C) 2 min, and (D) 3 min after seed addition. (E) STEM of an individual particle, (F) STEM-EDX elemental mapping of particle in (E) where yellow is Au, (G) TEM of an individual particle, and (H) EDX spectrum of the particle in (E). Signals from Cu, Fe, Co, and C are from the TEM grid/sample holder. No Pd peak is observed.

Differences in surface diffusion rates for the Au adatoms likely account for why Au seeds can adopt different shapes prior to branching and Pd seeds do not. The impact of diffusion rates on NC morphology development has been noted before.[18,32−34] For example, Xia *et al.* examined the impact of diffusion rates on the final morphology of Pd NCs prepared by a seeded method.[35] In particular, Pd precursor was injected into a solution containing 15 nm Pd nanocubes as seeds. At low temperature (0 °C), Pd nucleated at the vertices of the cubes and growth occurred only in ⟨111⟩ directions due to slow diffusion at low temperature. At high temperature (75 °C), cuboctahedral NCs formed due to diffusion and growth in the ⟨100⟩ and ⟨110⟩ directions. Thus, by adjusting diffusion rates, the final morphologies of the NCs could be controlled.

Considering the case of SMCR with Au seeds, this process can be represented by considering the diffusion of Au atoms on a Au surface.[22] In contrast, the case of SMCR with Pd seeds is represented by considering the diffusion of Au atoms on a Pd surface. Because of differences in lattice spacing and electronic structure, Au diffusion on Pd can be inferred to be slower than Au self-diffusion.[36,22] Thus, differences in diffusion rates are likely part of the explanation for why seeds of different compositions adopt different structures during overgrowth, ultimately resulting in differences in branched overgrowth.

With these diffusion properties in mind, a control study was conducted to manipulate diffusion of Au atoms on Pd seeds. In order to increase diffusion of Au

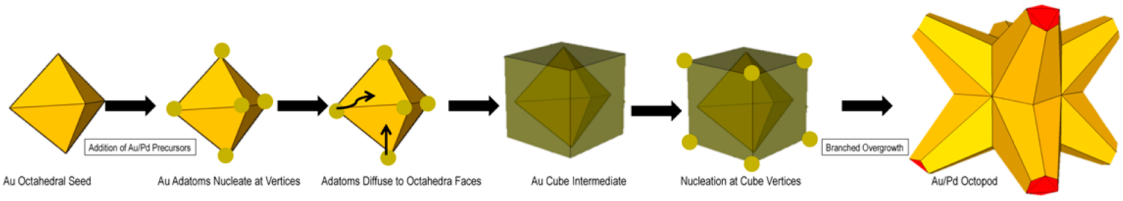

Scheme 1. A schematic describing the deposition of Au adatoms and subsequent diffusion on Au single-crystalline seeds from octahedra into cubes.

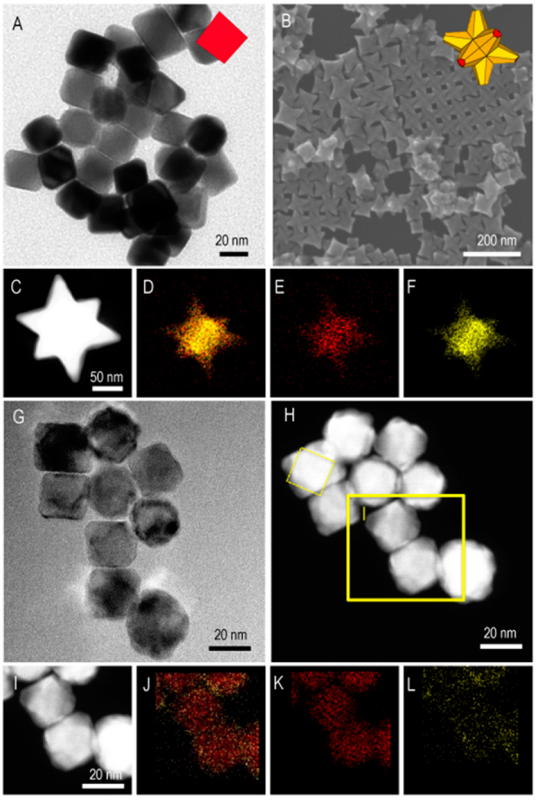

Figure 3. (A) SEM of octahedral Pd seeds. (B) SEM of Au/Pd octopods obtained *via* SMCR at 40 °C with octahedral Pd seeds. (C) STEM on an individual octopod, oriented with four branches in the plane, two out of the plane and two back into the plane (see model in part B). (D–F) STEM-EDX elemental mapping of the octopod where Au is represented by yellow and Pd is red; (D) is an overlay of Pd and Au signals, shown separately in (E) and (F). (G–L) Characterization of the product formation at 10 s after injection of Pd seeds. (G) TEM on core@shell Pd octahedra@Au cubic seeds. (H) STEM of the same seeds, where the octahedral core is evident. A dashed line box indicates a particle where the octahedral core is especially evident. The section mapped in (I–L) is indicated by a solid yellow box. (I–L) STEM-EDX elemental mapping of the NCs in (I) where Au is represented by yellow and Pd is red; (J) is an overlay of Pd and Au signals, shown separately in (K) and (L).

atoms on Pd seeds and induce a change in seed shape, SMCR with octahedral Pd seeds was performed at a higher temperature than the typical coreduction process. From 30 to 50 °C (the highest temperature studied), octopods were produced rather than the 24-branched NCs previously reported at room temperature (Figure S3, Supporting Information, row 1). Figure 3A–F shows SEM and STEM-EDX analysis of the resulting octopodal NCs synthesized at 40 °C. This structure is consistent with what is typically observed after SMCR with octahedral Au seeds and likely arises from Au adatoms diffusing on the octahedral Pd surface to adopt a cubic intermediate prior to branched overgrowth. To test this hypothesis, BSPP was used to quench the reaction in the earliest stages of overgrowth. As anticipated by the symmetry of the final product, nanostructures with cubic Au shells and octahedral Pd interiors were trapped as intermediates at ~10 s after Pd seed injection into growth solution at 40 °C. Figure 3G-H shows TEM and STEM/EDX analysis of the cubic intermediate with core@shell morphology.

It is important to note that by manipulating reaction temperature, the absorption strength of surfactants is manipulated as is the rate of precursor reduction. These system changes may also account for the differences between the room temperature and 40 °C experiments. Thus, to better understand the influence of temperature on morphology development, SMCR was performed at 30, 40, and 50 °C with Au octahedra as seeds for comparison; the results are the same as the typical room temperature synthesis with Au octahedra, with 8-branched octopods with O_h symmetry produced (Figure S3, Supporting Information, row 2). Although branched NCs are kinetic structural products, the formation of branches in all cases indicates that the changes in reaction rate with temperature do not perturb the overgrowth process substantially. Rather, small changes in temperature likely have a more substantial effect on the migration of atoms on the surface (which may or may not be mediated by the change in binding strength of the surfactants). This effect, in addition to facilitating changes in seed shape prior to branch growth, may account for the observed rounding of octopodal features and slight loss in sample uniformity at elevated temperatures. Complementary experiments below room temperature were also attempted. However, no conclusions could be drawn from these experiments due to the decrease in CTAB solubility. In addition to these temperature studies, Pd octahedra were heated at 40 °C overnight in either cetyltrimethylammonium chloride (CTAC)/NaBr or water; they maintained their octahedral shape after heating. Thus, the different morphology at 40 °C with octahedral Pd seeds cannot be accounted for by aging alone but rather the formation of cubic intermediates prior to branching *via* restructuring and/or overgrowth.

The formation of octopods at elevated temperatures supports the hypothesis that Pd cores maintain their shape during room-temperature SMCR due to lower surface diffusion rates of Au atoms on Pd surfaces compared to Au surfaces. To further test this hypothesis, SMCR with Au rhombic dodecahedra, synthesized from a literature protocol,[30] was examined. On the basis of results with Au octahedra and cubes as seeds, we hypothesized that octopods would form on account of cubic intermediate formation during overgrowth. Indeed, SEM, STEM, EDX, and electron diffraction analysis (Figure 1E–L) of the product support this hypothesis, with particles nearly identical to the Au/Pd octopods obtained with Au cubes and octahedra being produced. Electron diffraction confirmed that the branches grow in ⟨111⟩ directions. Still, even with the anticipated product obtained, this

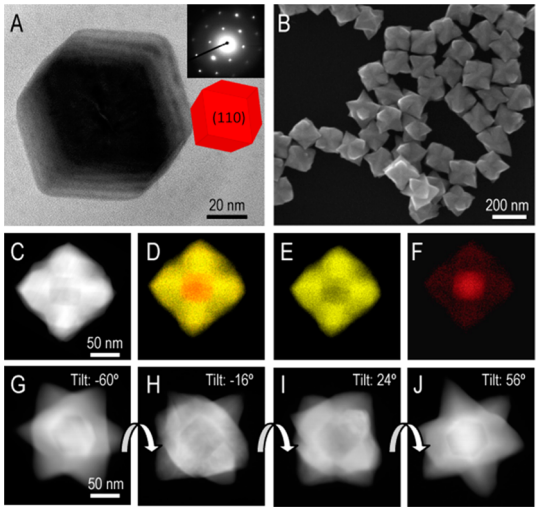

Figure 4. (A) TEM image of Pd rhombic dodecahedron (top inset: electron diffraction of the same particle). (B) SEM image of Au/Pd octopods from Pd rhombic dodecahedra. (C) STEM on an individual octopod built from a rhombic dodecahedral seed. (D−F) STEM-EDX elemental mapping of the octopod where Au is represented by yellow and Pd is red; (D) is an overlay of Au and Pd signals, shown separately in (E) and (F). (G−J) STEM tilt series of a Au/Pd octopod built from a Pd rhombic dodecahedron to reveal the structural relationship between the seed vertices and nanocrystal branches.

analysis is qualitative given the challenges associated with directly measuring diffusion on NCs and surfaces. Traditional methods require ultrahigh vacuum conditions, which would significantly deviate from our reaction conditions.[37] *In situ* TEM methods under development may provide an opportunity to observe this effect and quantify its contribution to morphology development.[38]

To contrast the deposition of Au/Pd onto rhombic dodecahedral Au seeds, SMCR was also performed with Pd rhombic dodecahedra as seeds. Figure 4A shows a TEM image of a typical Pd rhombic dodecahedron prepared by literature protocol.[39] The corresponding electron diffraction pattern (top right inset of Figure 4A) indicates that the particle is oriented in the [110] direction from the electron beam as shown in the model in the bottom right of Figure 4A. After SMCR, SEM images (Figure 4B) of the resultant branched structures reveal that the branching symmetry is the same as the Au-seed analogue, but the branches are much wider at the base than such octopodal samples (*e.g.*, Figure 1F).

Characterization by STEM (Figure 4C) indicates that the rhombic dodecahedral Pd seeds remain intact after SMCR. The two-dimensional (2-D) projection of this particle oriented along the [100] zone axis, confirmed by electron diffraction, is shown in Figure S4A,B (Supporting Information). This particle was also characterized by STEM-EDX elemental mapping (Figure 4D−F). On first examination, the shape of the Pd seed may appear cubic from the STEM image (Figure 4C); however, it is simply the rhombic dodecahedron lying on the substrate so that a vertex is oriented in the [100] zone axis. This orientation is depicted in Figure S2C−F (Supporting Information). This assignment is supported by the Pd map (Figure 4F), which reveals that the exterior of this seed is less enhanced with Pd compared to the interior. Additional STEM imaging provides corroborating evidence of a rhombic dodecahedral Pd interior with the hexagonal interior of an octopod oriented with two branches pointed away from the substrate, roughly the [110] orientation (Figure S4G, Supporting Information). The shape of the 2-D projection of the Pd seed in the STEM image is indicative of a rhombic dodecahedral interior and is not observed with octopods built from Pd nanocubes.[21]

One may expect more than eight branches from a rhombic dodecahedral Pd seed due to its 14 vertices. However, further investigations indicate that the branched overgrowth on Pd rhombic dodecahedra seeds is similar to what has been observed with other single-crystalline seeds. Rhombic dodecahedra have six vertices along ⟨100⟩ directions and eight vertices along ⟨111⟩ directions. These different vertices are denoted herein as V_{100} and V_{111}, respectively. To understand the overgrowth at the vertices, TEM and STEM images were acquired as a particle was tilted 30 degrees. This tilt series is reconstructed into a short movie, which is included in Video S1 (Supporting Information). Figure 4G−J shows 4 stills from the STEM tilt series which indicate that eight branches grow, one from each of the eight V_{111} along ⟨111⟩ directions of the rhombic dodecahedra. These results parallel those from Pd nanocubic seeds which yielded octopods, with one branch emerging from each V_{111} of a cube.[21] However, Pd rhombic dodecahedra also have six V_{100} which are maintained during SMCR. Growth in the ⟨111⟩ directions (along the edges of rhombic dodecahedral seeds) from one V_{100} would result in four branches, similar to growth of branches from the V_{100} of Pd octahedra.[21] Thus, additional growth from the V_{100} accounts for the enhanced branch thickness at the bases of these structures compared to octopods built from nanocubes. A summary scheme is provided as Figure S5 (Supporting Information).

This model of overgrowth is further supported by a study in which less metal was deposited onto the rhombic dodecahedral Pd seeds to reveal preferential sites for deposition before substantial branched overgrowth. As shown in Figure S6A−C (Supporting Information), NCs with more than eight branches are evident. In many cases, the particles orient with four branches toward the imaging substrate and four branches away from the imaging substrate. Additional overgrowth protrudes between each set of four branches but has yet to elongate. The orientation of these protrusions is better understood from the STEM imaging (Figure S6D,E, Supporting Information) in which the rhombic dodecahedral Pd seed is visible

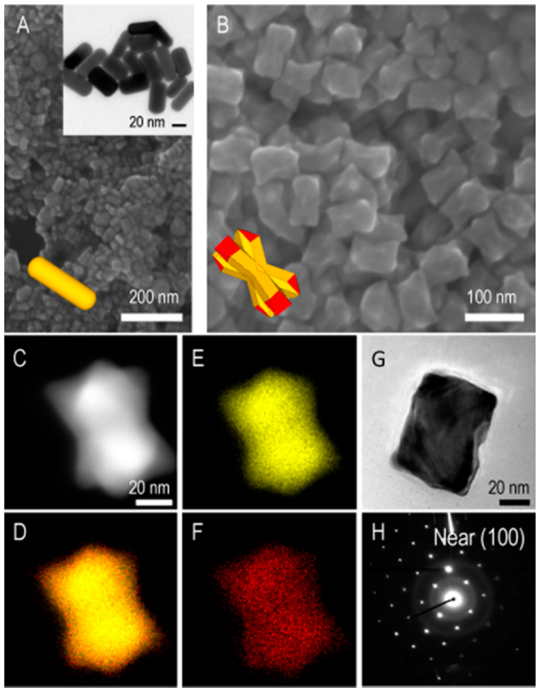

Figure 5. (A) SEM of short Au rod seeds. Inset: TEM. (B) SEM of Au/Pd octorods obtained from the seeds in (A). (C) STEM on an individual octorod. (D−F) STEM-EDX elemental mapping of an octorod where Au is represented by yellow and Pd is red; (F) is an overlay of Au and Pd signals, shown separately in (E) and (F). (G,H) TEM and corresponding electron diffraction.

and oriented as in the top of Figure S5 (Supporting Information). The eight dominant branches originate from the eight V_{111}, whereas the six protrusions correspond to overgrowth originating from the six V_{100}, which have yet to elongate or fuse with the eight dominant branches as suggested by Figure S5 (Supporting Information).

Coreduction with Anisotropic Seeds: The Case of Au Nanorods. In order to test whether or not single-crystalline Au seeds adopt {100}-terminated intermediates prior to branched growth more generally and to expand the symmetry classes of bimetallic nanostructures synthesized by SMCR, Au and Pd precursors were also coreduced to deposit metal onto short (43 ± 5 nm, aspect ratio ~2.3) and long (62 ± 7 nm, aspect ratio ~4.4) Au nanorods. These nanorods were synthesized from literature protocols,[40,41] are single-crystalline, and reported to be {250}-terminated. On the basis of the emerging guidelines, 8-branched nanoparticles with D_{4h} symmetry were anticipated. As shown in Figure 5, 8-branched NCs form that have D_{4h} symmetry, consistent with the elongated axis of the nanorod seed. From electron diffraction, branched growth was found to occur in ⟨111⟩ directions, similar to structures built from isotropic seeds. STEM-EDX and elemental mapping show that Au deposits primarily first onto the Au (shown in yellow) nanorods and Pd (shown in red) is localized at the tips. They are structurally similar to Au/Pd octopods, just elongated in the longitudinal direction. Huang *et al.* previously synthesized these structures *via* similar coreduction methods in the presence of Au nanorods.[15] SMCR with longer single-crystalline nanorods as seeds resulted in elongated octorods with similar morphology, which was confirmed by STEM-EDX and SEM (Figure S7, Supporting Information).

Interestingly, these results are similar to those previously obtained when Pd nanobars were used as seeds with SMCR.[21] Specifically, from {100}-terminated Pd nanobars, 8-branched Au/Pd bowties with D_{4h} symmetry were obtained. Elemental analysis by STEM-EDX of these structures revealed that one branch emerges per each vertex of the seed and proceed in ⟨111⟩ directions. The similarities between products obtained with Au nanorod seeds and Pd nanobars support the hypothesis that the {250}-terminated Au nanorods adopt {100}-terminated intermediates prior to branched growth. These results are also consistent with the results obtained with isotropic single-crystalline Au NC seeds, which yielded 8-branched NCs upon SMCR.

Finally, as Au nanorods are synthesized in the presence of a small amount of Ag^+, which remains adsorbed to their surfaces,[42] a control experiment of SMCR on Au concave cubes was performed to evaluate if Ag^+ could contribute to the final morphologies. The hypothesis is that single-crystalline Au seeds generate Au/Pd octopods upon coreduction. Thus, if Ag^+ has no effect on final morphology, then octopods should be the product. Au and Pd precursors were coreduced to deposit metal onto single-crystalline Au concave cubes;[43] the result was octopods (Figure S11, Supporting Information). These results support that small concentrations of Ag^+ on the surface of the Au cores do not affect the final morphology of the branched product; however, the unavailability of other single-crystalline Au seeds prepared in the presence of Ag^+ precludes a full examination of this parameter.

Coreduction with Twinned NC Seeds. These studies find that when building NCs from single-crystalline Au seeds *via* SMCR, a limited number of branch symmetries are accessible because diffusion drives single-crystalline Au seeds to adopt {100}-terminated intermediates. Switching to Pd seeds provides new branching patterns as the selected seed shape is preserved until branched growth initiates. However, depending on the intended use of the NCs, a Pd interior may not be preferred.[21] Thus, we sought to expand the classes of branched nanostructures though the use of seeds with twin planes and thus different shapes. Previously, Au and Pd precursors were coreduced to deposit metal onto {100}-terminated Pd right bipyramids, which contain a (111) twin plane, and 5-branched pentapods with D_{3h} symmetry are the major product.[21] In this case, two axial branches proceed along ⟨111⟩ directions and three equatorial branches proceed along ⟨112⟩ directions,

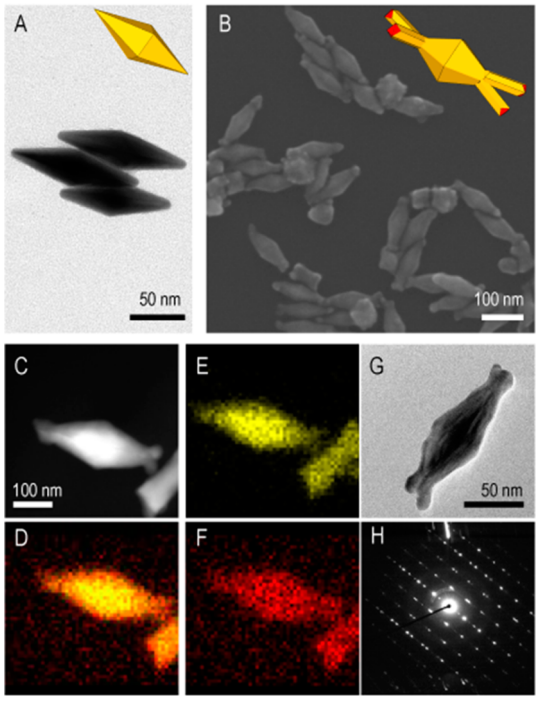

Figure 6. (A) TEM of penta-twinned Au bipyramid seeds. (B) SEM of Au/Pd branched NCs built from seeds shown in (A). (C) STEM of an individual NC. (D–F) STEM-EDX elemental mapping of an NC where Au is represented by yellow and Pd is red, (D) is an overlay of Au and Pd signals, shown separately in (E) and (F). (G,H) TEM and corresponding electron diffraction.

with the twin plane from the right bipyramidal seeds conserved within the equatorial branches. However, SMCR has not been applied to shape-controlled Au seeds containing twin panes but may yield new branching patterns.

For example, pentagonally twinned Au bipyramids[44] were used as seeds for the synthesis of Au/Pd nanostructures by SMCR. It was hypothesized that five branches would grow from each end of a bipyramid due to the penta-twinned nature of the seeds; however, only two or three branches were found to grow off each end of the bipyramid. Moreover, no branches emerged from the obtuse vertices around the center of the bipyramids, likely due to their large angle (Figure 6). Electron diffraction displayed five overlapping patterns instead of one due to the penta-twinned nature of the cores and orientation of the particles relative to the electron beam. Thus, assignment of the branch directions was challenging, and a back of the envelope calculation was used to assist in assignment. That is, the twin plane through the center of the particle is (110) and that plane is bisected at a 90° angle by each of the longitudinal penta-twinned planes. From a TEM tilt study (Figure S9, Video S2, Supporting Information), the angle between the longitudinal twin plane and the branch was measured to be approximately 140°. Therefore, the angle between the branch and the (110) plane is approximately 50°. The angle between (111) and (110) planes in an FCC metal is 54°, which is close to 50° (see Figure S10, Supporting Information). Therefore, branched overgrowth in twinned Au nanostructures likely proceeds in a similar manner to Pd NCs as seeds; however, the maximum number of branches is not realized with these seeds.

In addition to pentagonally twinned Au bipyramids, SMCR was performed using Au decahedra[45] and triangular nanoplates as seeds (the latter of which are impurities in the synthesis of Au decahedra and contain stacking faults). Figure S11 (Supporting Information) displays SEM images of branched NCs after SMCR on Au decahedra and nanoplates. Two types of particles are observed; the first are elongated NCs with 10 miniature branches and the second have six in-plane branches. We anticipate that these seeds follow similar growth patterns; however, due to their structural complexity, growth directions are difficult to assign with certainty. For decahedra, the seeds increase in length during overgrowth, similar to Au nanorods from decahedral seeds (Figure S10, Video S3, Supporting Information).[46] With this elongation, branches also grow from the vertices in ⟨111⟩ directions for a total of 10 small branches. This result was expected, as branches grow from each of the five vertices. However, seed elongation has not been previously observed and likely arises on account of the twinned nature of the seeds in which lateral growth would increase strain within the NCs.[47] In the case of triangular plate impurities, SMCR results in particles with six branches (Figure S10, Video S4, Supporting Information). Literature results indicate that triangular Au plates can evolve into hexagonal plates with the addition of reducing agent and $AuCl_4^-$.[48,49] Similarly, the triangular plates become hexagonal plates with six vertices during SMCR. The particles are not perfectly hexagonal as evidenced in Figure S11 (Supporting Information), and this difference can be attributed to branched overgrowth before full transformation to hexagonal plates. Regardless, with the inclusion of twin planes or stacking faults, new structural complexity is evident in the branched NCs synthesized by SMCR.

CONCLUSIONS

SMCR has proven to be versatile, as previously core@shell Au@alloy Au/Pd octahedra and nanocrystals with a hopper-like morphology were achieved by manipulating pH and bromide concentration, respectively.[18] Here, these studies of SMCR on single-crystalline, anisotropic, and twinned Au and Pd seeds provide rules for the rational design of branched NCs as functions of seed shape and composition. Single-crystalline Au seeds yield 8-branched octopods, which are in contrast to Pd seeds, which demonstrate growth in ⟨111⟩ directions from the high-energy vertices. These results are consistent with Au seeds adopting cubic intermediates prior to branch growth on account

of rapid self-diffusion of Au atoms on Au seeds compared to slower diffusion of Au atoms on Pd seeds. After formation of {100}-terminated intermediates from Au seeds, metal addition occurs on each of the eight vertices to yield octopods. In twinned structures, branches grow from vertices, but may not necessarily proceed in ⟨111⟩ directions. Thus, far, the following rules for branched growth *via* SMCR have been determined:

(1) *There are symmetry relationships between NC seeds and the stellated nanostructures grown from them, with overgrowth occurring preferentially from the high-energy vertices of the seeds under kinetically controlled growth conditions.* This guideline is based primarily on SMCR experiments using shape-controlled Pd NCs from which elemental mapping of product particles revealed the emergence of branches from the vertices of the seeds.[21]

(2) *To use these symmetry relationships, seeds must be structurally stable and not adopt a new shape prior to branch formation. Structural instability is common when Au deposits on Au seeds but can be inhibited by selecting heterodeposition systems.* This guideline is based on SMCR experiments with single-crystalline {100}-terminated Au nanocubes, {110}-terminated Au rhombic dodecahedra, and {111}-terminated Au octahedra, which resulted in 8-branched octopods. These results contrast with SMCR on single-crystalline Pd seeds.

(3) *Branches proceed in ⟨111⟩ directions from seeds without internal twinning; twinned seeds can yield nanostructures with unexpected symmetries.* More than one branch may grow from each vertex, provided branches grow in energetically equal ⟨111⟩ directions. The use of twinned seeds can provide NCs with branching patterns difficult to predict. For example, our previous studies with Pd right bipyramids[21] as seeds yielded NCs with branches in ⟨112⟩ directions. Studies with pentagonally twinned Au bipyramids as seeds revealed that not all vertices will yield branches. Thus, the maximum number of branches does not always grow from the vertices of twinned seeds.

(4) *These guidelines apply also to anisotropic structures.* This guideline is based on studies with Pd bars[21] and single-crystalline Au nanorods as seeds. These studies confirmed that branched growth occurs preferentially from seed vertices and that anisotropic Au seeds can adopt new shapes prior to branch overgrowth.

Harnessing these rules will aid in further design of new nanostructures with different bimetallic compositions and function.[50−52]

METHODS

See Supporting Information for chemicals, characterization methods, and detailed description of synthetic techniques. In short, shape-controlled Au or Pd NCs were synthesized by previous literature methods for use as seeds. Seeds include Au nanocubes, Au octahedra, Au rhombic dodecahedra, short Au rods, long Au rods, penta-twinned Au bipyramids, Au decahedra as well as Pd octahedra and Pd rhombic dodecahedra. For branched nanocrystal growth *via* SMCR, typically, 2 mL of CTAB (0.2 M) solution was added to a reaction vial. Next, 0.1 mL of H_2PdCl_4 (10 mM) solution and 0.1 mL of $HAuCl_4 \cdot 3H_2O$ (0.1 M) solution were added followed by 1.5 mL of L-ascorbic acid (0.1 M). In the absence of seeds, the reduction of the precursors with L-ascorbic acid is slow, and thus self-nucleation is inhibited. Then 21.4 mL of water was added, followed by a solution of selected shape-controlled seeds. These reaction vials were gently shaken then capped and allowed to sit undisturbed in a 25 °C oil bath for 2−24 h. Reaction conditions were optimized by modifying the ratio of Au-to-Pd precursor and seed volume for each system due to variation in seed size and surface structure.[14] Complete synthetic details for each sample can be found in Table S1 (Supporting Information).

Conflict of Interest: The authors declare no competing financial interest.

Acknowledgment. The authors would like to thank the IU Nanoscale Characterization Facility for access to instrumentation. This work was supported by start-up funds from Indiana University and now NSF Award CHE-1306853. Cardoso supported by an Academic Merit fellowship from Universidade de Sao Paulo. Skrabalak is a Cottrell Scholar (Research Corporation), Sloan Research Fellow, and Camille Dreyfus Teacher-Scholar.

Supporting Information Available: Experimental procedures, additional materials characterization, and movies from TEM tilt studies. This material is available free of charge *via* the Internet at http://pubs.acs.org.

REFERENCES AND NOTES

1. Xia, Y.; Xiong, Y.; Lim, B.; Skrabalak, S. E. Shape-Controlled Synthesis of Metal Nanocrystals: Simple Chemistry Meets Complex Physics? *Angew. Chem., Int. Ed.* **2009**, *48*, 60–103.
2. Ringe, E.; Sharma, B.; Henry, A.-I.; Marks, L. D.; Van Duyne, R. P. Single Nanoparticle Plasmonics. *Phys. Chem. Chem. Phys.* **2013**, *15*, 4110–4129.
3. Grzelczak, M.; Liz-Marzán, L. M. Colloidal Nanoplasmonics: From Building Blocks to Sensing Devices. *Langmuir* **2013**, *29*, 4652–4663.
4. Mahmoud, M. A.; O'Neil, D.; El-Sayed, M. A. Hollow and Solid Metallic Nanoparticles in Sensing and in Nanocatalysis. *Chem. Mater.* **2013**, *26*, 44–58.
5. Lim, B.; Xia, Y. Metal Nanocrystals with Highly Branched Morphologies. *Angew. Chem., Int. Ed.* **2011**, *50*, 76–85.
6. DeSantis, C. J.; Weiner, R. G.; Radmilovic, A.; Bower, M. M.; Skrabalak, S. E. Seeding Bimetallic Nanostructures as a New Class of Plasmonic Colloids. *J. Phys. Chem. Lett.* **2013**, 3072–3082.
7. Chen, H.; Wang, F.; Li, K.; Woo, K. C.; Wang, J.; Li, Q.; Sun, L.-D.; Zhang, X.; Lin, H.-Q.; Yan, C.-H. Plasmonic Percolation: Plasmon-Manifested Dielectric-to-Metal Transition. *ACS Nano* **2012**, *6*, 7162–7171.
8. Suntivich, J.; Xu, Z.; Carlton, C. E.; Kim, J.; Han, B.; Lee, S. W.; Bonnet, N.; Marzari, N.; Allard, L. F.; Gasteiger, H. A.; *et al.* Surface Composition Tuning of Au−Pt Bimetallic Nanoparticles for Enhanced Carbon Monoxide and Methanol Electro-oxidation. *J. Am. Chem. Soc.* **2013**, *135*, 7985–7991.
9. Mazumder, V.; Chi, M.; More, K. L.; Sun, S. Synthesis and Characterization of Multimetallic Pd/Au and Pd/Au/FePt Core/Shell Nanoparticles. *Angew. Chem., Int. Ed.* **2010**, *49*, 9368–9372.
10. Lim, B.; Jiang, M.; Camargo, P. H. C.; Cho, E. C.; Tao, J.; Lu, X.; Zhu, Y.; Xia, Y. Pd-Pt Bimetallic Nanodendrites with High Activity for Oxygen Reduction. *Science* **2009**, *324*, 1302–1305.

11. Guo, X.; Zhang, Q.; Sun, Y.; Zhao, Q.; Yang, J. Lateral Etching of Core−Shell Au@Metal Nanorods to Metal-Tipped Au Nanorods with Improved Catalytic Activity. *ACS Nano* **2012**, *6*, 1165–1175.
12. Hong, J. W.; Kim, D.; Lee, Y. W.; Kim, M.; Kang, S. W.; Han, S. W. Atomic-Distribution-Dependent Electrocatalytic Activity of Au−Pd Bimetallic Nanocrystals. *Angew. Chem., Int. Ed.* **2011**, *50*, 8876–8880.
13. Zhou, S.; Jackson, G. S.; Eichhorn, B. AuPt Alloy Nanoparticles for CO-Tolerant Hydrogen Activation: Architectural Effects in Au-Pt Bimetallic Nanocatalysts. *Adv. Funct. Mater.* **2007**, *17*, 3099–3104.
14. DeSantis, C. J.; Peverly, A. A.; Peters, D. G.; Skrabalak, S. E. Octopods *versus* Concave Nanocrystals: Control of Morphology by Manipulating the Kinetics of Seeded Growth *via* Co-Reduction. *Nano Lett.* **2011**, *11*, 2164–2168.
15. Huang, J.; Zhu, Y.; Lin, M.; Wang, Q.; Zhao, L.; Yang, Y.; Yao, K. X.; Han, Y. Site-Specific Growth of Au−Pd Alloy Horns on Au Nanorods: A Platform for Highly Sensitive Monitoring of Catalytic Reactions by Surface Enhancement Raman Spectroscopy. *J. Am. Chem. Soc.* **2013**, *135*, 8552–8561.
16. Chen, S.; Jenkins, S. V.; Tao, J.; Zhu, Y.; Chen, J. Anisotropic Seeded Growth of Cu−M (M = Au, Pt, or Pd) Bimetallic Nanorods with Tunable Optical and Catalytic Properties. *J. Phys. Chem. C* **2013**, *117*, 8924–8932.
17. Kim, D.; Lee, Y. W.; Lee, S. B.; Han, S. W. Convex Polyhedral Au@Pd Core−Shell Nanocrystals with High-Index Facets. *Angew. Chem., Int. Ed.* **2012**, *51*, 159–163.
18. DeSantis, C. J.; Sue, A. C.; Bower, M. M.; Skrabalak, S. E. Seed-Mediated Co-reduction: A Versatile Route to Architecturally Controlled Bimetallic Nanostructures. *ACS Nano* **2012**, *6*, 2617–2628.
19. DeSantis, C. J.; Skrabalak, S. E. Size-Controlled Synthesis of Au/Pd Octopods with High Refractive Index Sensitivity. *Langmuir* **2012**, *28*, 9055–9062.
20. Langille, M. R.; Zhang, J.; Personick, M. L.; Li, S.; Mirkin, C. A. Stepwise Evolution of Spherical Seeds into 20-Fold Twinned Icosahedra. *Science* **2012**, *337*, 954–957.
21. DeSantis, C. J.; Skrabalak, S. E. Core Values: Elucidating the Role of Seed Structure in the Synthesis of Symmetrically Branched Nanocrystals. *J. Am. Chem. Soc.* **2012**, *135*, 10–13.
22. Neumann, G.; Tuijn, C. Self-Diffusion and Impurity Diffusion in Pure Metals: Handbook of Experimental Data. In *Pergamon Materials Series*; Gerhard, N., Cornelis, T., Eds.; Pergamon: Oxford, 2008; Vol. 14.
23. Self-Diffusion in Metals. In *Diffusion in Solids*; Springer: Berlin, 2007; Vol. 155, pp 297−312.
24. Dovgolevsky, E.; Haick, H. Direct Observation of the Transition Point Between Quasi-Spherical and Cubic Nanoparticles in a Two-Step Seed-Mediated Growth Method. *Small* **2008**, *4*, 2059–2066.
25. Zhang, J.; Langille, M. R.; Mirkin, C. A. Photomediated Synthesis of Silver Triangular Bipyramids and Prisms: The Effect of pH and BSPP. *J. Am. Chem. Soc.* **2010**, *132*, 12502–12510.
26. Lim, B.; Jiang, M.; Tao, J.; Camargo, P. H. C.; Zhu, Y.; Xia, Y. Shape-Controlled Synthesis of Pd Nanocrystals in Aqueous Solutions. *Adv. Funct. Mater.* **2009**, *19*, 189–200.
27. Bower, M. M.; DeSantis, C. J.; Skrabalak, S. E. A Quantitative Analysis of Anions and pH on the Growth of Bimetallic Nanostructures. *J. Phys. Chem. C* **2014**, 10.1021/jp5053776.
28. Park, Y.; Lee, Y. W.; Kang, S. W.; Han, S. W. One-Pot Synthesis of Au@Pd Core-Shell Nanocrystals with Multiple High- and Low-Index Facets and Their High Electrocatalytic Performance. *Nanoscale* **2014**, *6*, 9798–9805.
29. Surrey, A.; Pohl, D.; Schultz, L.; Rellinghaus, B. Quantitative Measurement of the Surface Self-Diffusion on Au Nanoparticles by Aberration-Corrected Transmission Electron Microscopy. *Nano Lett.* **2012**, *12*, 6071–6077.
30. Wu, H.-L.; Kuo, C.-H.; Huang, M. H. Seed-Mediated Synthesis of Gold Nanocrystals with Systematic Shape Evolution from Cubic to Trisoctahedral and Rhombic Dodecahedral Structures. *Langmuir* **2010**, *26*, 12307–12313.
31. Laskar, M.; Zhong, X.; Li, Z.-Y.; Skrabalak, S. E. Manipulating the Kinetics of Seeded Growth for Edge-Selective Metal Deposition and the Formation of Concave Au Nanocrystals. *ChemSusChem* **2013**, *6*, 1959–1965.
32. Yin, Y.; Rioux, R. M.; Erdonmez, C. K.; Hughes, S.; Somorjai, G. A.; Alivisatos, A. P. Formation of Hollow Nanocrystals Through the Nanoscale Kirkendall Effect. *Science* **2004**, *304*, 711–714.
33. Peng, X.; Wickham, J.; Alivisatos, A. P. Kinetics of II-VI and III-V Colloidal Semiconductor Nanocrystal Growth: "Focusing" of Size Distributions. *J. Am. Chem. Soc.* **1998**, *120*, 5343–5344.
34. Horiguchi, Y.; Honda, K.; Kato, Y.; Nakashima, N.; Niidome, Y. Photothermal Reshaping of Gold Nanorods Depends on the Passivating Layers of the Nanorod Surfaces. *Langmuir* **2008**, *24*, 12026–12031.
35. Xia, X.; Xie, S.; Liu, M.; Peng, H.-C.; Lu, N.; Wang, J.; Kim, M. J.; Xia, Y. On the Role of Surface Diffusion in Determining the Shape or Morphology of Noble-Metal Nanocrystals. *Proc. Natl. Acad. Sci. U. S. A.* **2013**, *110*, 6669–6673.
36. Dill, K. A.; Bromberg, S. *Molecular Driving Forces: Statistical Thermodynamics in Biology, Chemistry, Physics, and Nanoscience*; Taylor & Francis Group: New York, 2011.
37. Somorjai, G. A.; Li, Y. *Introduction to Surface Chemistry and Catalysis*; John Wiley & Sons: Hoboken, 2010.
38. Evans, J. E.; Jungjohann, K. L.; Browning, N. D.; Arslan, I. Controlled Growth of Nanoparticles from Solution with *In Situ* Liquid Transmission Electron Microscopy. *Nano Lett.* **2011**, *11*, 2809–2813.
39. Niu, W.; Zhang, L.; Xu, G. Shape-Controlled Synthesis of Single-Crystalline Palladium Nanocrystals. *ACS Nano* **2010**, *4*, 1987–1996.
40. Ye, X.; Jin, L.; Caglayan, H.; Chen, J.; Xing, G.; Zheng, C.; Doan-Nguyen, V.; Kang, Y.; Engheta, N.; Kagan, C. R.; *et al.* Improved Size-Tunable Synthesis of Monodisperse Gold Nanorods through the Use of Aromatic Additives. *ACS Nano* **2012**, *6*, 2804–2817.
41. Vigderman, L.; Zubarev, E. R. High-Yield Synthesis of Gold Nanorods with Longitudinal SPR Peak Greater than 1200 nm Using Hydroquinone as a Reducing Agent. *Chem. Mater.* **2013**, *25*, 1450–1457.
42. Jackson, S. R.; McBride, J. R.; Rosenthal, S. J.; Wright, D. W. Where's the Silver? Imaging Trace Silver Coverage on the Surface of Gold Nanorods. *J. Am. Chem. Soc.* **2014**, *136*, 5261–5263.
43. Langille, M. R.; Personick, M. L.; Zhang, J.; Mirkin, C. A. Defining Rules for the Shape Evolution of Gold Nanoparticles. *J. Am. Chem. Soc.* **2012**, *134*, 14542–14554.
44. Liu; Guyot-Sionnest, P. Mechanism of Silver(I)-Assisted Growth of Gold Nanorods and Bipyramids. *J. Phys. Chem. B* **2005**, *109*, 22192–22200.
45. Sun, J.; Guan, M.; Shang, T.; Gao, C.; Xu, Z.; Zhu, J. Selective Synthesis of Gold Cuboid and Decahedral Nanoparticles Regulated and Controlled by Cu^{2+} Ions. *Cryst. Growth Des.* **2008**, *8*, 906–910.
46. Murphy, C. J.; Thompson, L. B.; Alkilany, A. M.; Sisco, P. N.; Boulos, S. P.; Sivapalan, S. T.; Yang, J. A.; Chernak, D. J.; Huang, J. The Many Faces of Gold Nanorods. *J. Phys. Chem. Lett.* **2010**, *1*, 2867–2875.
47. Jana, N. R.; Gearheart, L.; Murphy, C. J. Wet Chemical Synthesis of High Aspect Ratio Cylindrical Gold Nanorods. *J. Phys. Chem. B* **2001**, *105*, 4065–4067.
48. Hong, S.; Shuford, K. L.; Park, S. Shape Transformation of Gold Nanoplates and their Surface Plasmon Characterization: Triangular to Hexagonal Nanoplates. *Chem. Mater.* **2011**, *23*, 2011–2013.
49. Hong, S.; Acapulcoaaa, J. A. I.; Jang, H. Y.; Park, S. Au Nanodisk-Core Multishell Nanoparticles: Synthetic Method for Controlling Number of Shells and Intershell Distance. *Chem. Mater.* **2014**, *26*, 3618–3623.
50. Yang, Y.; Zhang, Q.; Fu, Z.-W.; Qin, D. Transformation of Ag Nanocubes into Ag−Au Hollow Nanostructures with Enriched Ag Contents to Improve SERS Activity and Chemical Stability. *ACS Appl. Mater. Interfaces* **2014**, *6*, 3750–3757.
51. Heck, K. N.; Janesko, B. G.; Scuseria, G. E.; Halas, N. J.; Wong, M. S. Observing Metal-Catalyzed Chemical Reactions *In Situ* Using Surface-Enhanced Raman Spectroscopy on

Pd−Au Nanoshells. *J. Am. Chem. Soc.* **2008**, *130*, 16592–16600.
52. Liu, R.; Liu, J.-F.; Zhang, Z.-M.; Zhang, L.-Q.; Sun, J.-F.; Sun, M.-T.; Jiang, G.-B. Submonolayer-Pt-Coated Ultrathin Au Nanowires and Their Self-Organized Nanoporous Film: SERS and Catalysis Active Substrates for *Operando* SERS Monitoring of Catalytic Reactions. *J. Phys. Chem. Lett.* **2014**, *5*, 969–975.